Magnetic order and crystal structure in the superconducting $R\mathrm{Ni_2B_2C}$ materials

J. W. Lynn and S. Skanthakumar
Reactor Radiation Division, National Institute of Standards and Technology, Gaithersburg, Maryland 20899 and Center for Superconductivity Research, University of Maryland, College Park, Maryland 20742

Q. Huang
Reactor Radiation Division, National Institute of Standards and Technology, Gaithersburg, Maryland 20899 and Materials Engineering Program, University of Maryland, College Park, Maryland 20742

S. K. Sinha
Advanced Photon Source, Argonne National Laboratory, Argonne, Illinois 60439

Z. Hossain, L. C. Gupta, and R. Nagarajan
Tata Institute of Fundamental Research, Bombay 400 005, India

C. Godart
CNRS, UPR-209, 92195 Meudon, France
(Received 27 September 1996)

Neutron-diffraction measurements have been carried out to investigate the crystal structure, magnetic structures, and magnetic phase transitions in $R\mathrm{Ni_2B_2C}$ ($R=$ Y, Ce, Pr, Nd, Tb, Dy, Ho, Er, Tm, and Yb). The materials that order magnetically exhibit a wide variety of both commensurate and incommensurate magnetic structures, which argues strongly that the dominant exchange interactions are of the indirect Ruderman-Kittel-Kasuya-Yosida type. The Nd system exhibits a commensurate antiferromagnetic ordering at 4.8 K, with wave vector $\delta=(1/2,0,1/2)$ and moment direction along a (or equivalently with $\delta=(0,1/2,1/2)$ and moment direction along b in this tetragonal system). For Dy ($T_N=10.6$ K), Pr ($T_N=4.0$ K), and the low-temperature phase of Ho, the magnetic structure is also a commensurate antiferromagnet that consists of ferromagnetic sheets of rare-earth moments in the a-b plane, with the sheets coupled antiferromagnetically along the c axis [$\delta=(0,0,1)$]. Pr is not superconducting, while for Dy ($T_c=6$ K) and Ho ($T_c=8$ K) this magnetic order coexists with superconductivity. For Ho, though, the magnetic state that initially forms at $T_N\approx 8.5$ K is an incommensurate spiral antiferromagnetic state along the c axis in which the direction of these ferromagnetic sheets are rotated in the a-b plane by $\sim 17°$ from their low-temperature antiparallel configuration [$\delta=(0,0,0.91)$]. The intensity for this spiral state reaches a maximum near the reentrant superconducting transition (~ 5 K); the spiral state then collapses at lower temperature in favor of the commensurate antiferromagnetic state. An incommensurate a-axis modulation, with $\delta=(0.55,0,0)$, is also observed above the spiral-antiferromagnetic transition, but it exists over a narrower temperature range than the spiral state, and also collapses near the reentrant superconducting transition. The Er system forms an incommensurate, transversely polarized spin-density wave (SDW) state at $T_N=6.8$ K, with $\delta=(0.553,0,0)$ and moment direction along b (or with δ along b and the moment direction along a). The SDW squares up at low T, and coexists with the superconducting state ($T_c=11$ K) over the full temperature range where magnetic order is present. Tb, which does not superconduct, orders with a very similar wave vector, but the SDW is longitudinally polarized in this case and again squares up at low T. Tm orders at $T_N=1.5$ K in a transversely polarized SDW state, but with the moments along the c axis and $\delta=(0.093,0.093,0)$. This state is coexistent with superconductivity ($T_c=11$ K). No significant magnetic moment is found to develop on the Ni site in any of the materials, and there is no magnetic ordering of any kind in the Y, Yb, or Ce materials. Profile refinements have also been carried out on these same samples to investigate the systematics of the crystallography, and the crystal structure is $I4/mmm$ over the full range of compositions and temperatures investigated. The area of the a-b plane and the volume of the unit cell both decrease smoothly with either decreasing lanthanide radius or decreasing temperature, but the strong boron-carbon and nickel-carbon bonding then forces the c axis to expand. [S0163-1829(97)06010-4]

I. INTRODUCTION

The properties of the new classes of quaternary intermetallic superconductors such as the borocarbide series $R\mathrm{Ni_2B_2C}$ and RNiBC (R = rare-earth ion)[1–4] have attracted a great deal of attention recently because of their interesting superconducting and magnetic properties, and the interaction between the two. From the viewpoint of their superconductivity properties these systems have relatively high transition temperatures (up to 23 K for $\mathrm{YPd_2B_2C}$),[2] and are the first

quaternary intermetallic systems that are superconducting. Initially they were also thought to be the first ''high-T_c'' materials that do not contain either copper or oxygen. However, it quickly became apparent from measurements of the physical properties as well as band-structure calculations[5] that these new materials are three-dimensional in their behavior, and thus are in fact quite different than the layered cuprates. The substantial isotope effect,[6] the nature of the electronic properties,[7] as well as theoretical calculations, all show that the electron-phonon interaction is strong in these systems, and the high T_c's are now thought to originate from a peak in the electronic density of states at the Fermi surface. The strong suppression of the superconducting transition temperature with magnetic doping onto the Ni lattice[8] also indicates that these are conventional electron-phonon superconductors. More recently, a phonon anomaly, reminiscent of the strong electron-phonon coupling found previously in carbide superconductors and related systems,[9] has also been observed in this class of materials,[10] and very recently an additional lattice-dynamical mode directly associated with the formation of the superconducting state has been discovered.[11] It therefore is apparent that these materials are model electron-phonon superconductors.

The interaction between magnetic long-range order and superconductivity has been an active area of interest for many years, and in this regard these new quaternary materials play a unique role. In the ternary Chevrel-phase and related magnetic-superconductor systems[12] the magnetic ordering temperatures are typically ~ 1 K, comparable to the expected dipolar ordering temperatures. Magnetic exchange interactions play a role in determining the magnetic structures that are realized, but at most they are comparable to the dipole interactions, and the magnetic ordering temperatures are typically much lower than the superconducting transitions. An even more extreme situation is found for the high-T_c cuprate superconductors, where the rare-earth ions again become ordered in the 1 K range,[13] while the superconducting transitions are one to two orders-of-magnitude higher in temperature.

Following the initial discovery of the quaternary materials, Eisaki *et al.*[14] investigated the systematics of rare-earth substitution in the system. They found that almost all the rare earths ordered magnetically, and that many were superconducting as well. The magnetic ordering temperatures occur at much higher temperatures [with T_N as high as 19 K for $GdNi_2B_2C$, (Refs. 15 and 16)] than for the Chevrel phase or cuprate materials, while the superconducting transition temperatures (when they occur) are comparable to the magnetic transition temperatures. The much higher Néel temperatures ensure that the magnetic energetics for these new systems are dominated by exchange rather than dipolar (electromagnetic) interactions, while the comparable superconducting condensation energies ensure that the interplay between superconductivity and magnetism should be much stronger than for the earlier systems and on a comparable energetic footing. This has indeed turned out to be the case, with the most interesting system appearing to be $HoNi_2B_2C$. This material becomes superconducting at ~ 8 K, then reenters the normal state at ~ 5 K, only to quickly become superconducting again with further reduction of temperature.[14,17] The first neutron studies revealed that coincidently with the superconductivity, long-range magnetic order develops at about the same temperature.[18,19] Two types of magnetic order were initially observed; a commensurate antiferromagnetic structure that consists of sheets of ferromagnetic moments in the a-b plane, with adjacent sheets coupled antiferromagnetically along the c axis, and an incommensurate spiral state that is obtained by rotating the direction of these ferromagnetic sheets in the a-b plane by an angle $\phi = 16.6°$ away from the antiferromagnetic arrangement. If this angle were exactly 15° then this would be a long-wavelength commensurate spiral, with a period of 24 Ho layers (12 unit cells). However, the actual spiral that forms is incommensurate with the underlying lattice. The intensities from both types of Bragg peaks develop at about the same ordering temperature and initially grow with decreasing temperature at the same rate. At ~ 5 K the superconductivity is reentrant as evidenced by a deep minimum in H_{c2} near 5 K,[14] below which the incommensurate spiral order locks into the commensurate antiferromagnetic structure. An additional incommensurate magnetic component, with wave vector along the a axis, was found to develop at a lower temperature (~ 6 K), and this component also disappears near the reentrant transition.[20,21] Once the system is in the commensurate antiferromagnetic state, this permits the return of superconductivity, and the long-range antiferromagnetic order coexists with superconductivity at low temperatures.

The nature of the magnetic order and its influence on the superconductivity is clearly quite interesting in these RNi_2B_2C materials, and here we report a systematic investigation of the magnetic structures and phase transitions across the rare-earth series. There is quite a variety of magnetic structures found for the different rare earths. Some are relatively simple commensurate antiferromagnets, while others form incommensurate structures with modulation wave vectors that are sometimes along the [100] direction, sometimes along the [110] direction, and sometimes along the [001] direction. This behavior is reminiscent of the rare-earth elemental systems,[22] and argues that the exchange interactions are of the Rudermen-Kittel-Kasuya-Yosida (RKKY) type, mediated through the conduction electrons. We have also found, as others have,[23] that the magnetic and superconducting properties are very sensitive functions of the composition. We therefore have also carried out a systematic study of the crystal structure of our samples in order to establish the systematics and identify if possible the underlying property that is controlling this very subtle dependence on composition.

II. EXPERIMENTAL PROCEDURES

Polycrystalline samples of RNi_2B_2C (R= Y, Ce, Pr, Nd, Tb, Dy, Ho, Er, Tm) were prepared using a standard arc melting technique under flowing argon atmosphere. Starting materials were high purity (about 99.9% or better) elements in the form of chips, wire or thin rods. First the stoichiometric amounts of R, Ni, and B were taken and melted on the water-cooled copper hearth of the arc furnace under flowing argon atmosphere. A titanium piece was used as a getter for oxygen. Any weight loss after the first melting of the sample was attributed to boron and was accordingly compensated. The sample was melted once more and again

checked for weight loss. Then the RNi_2B_2 alloy button was melted along with carbon which was taken either as a felt (99.7% pure) or pieces from a graphite rod (99.99% pure). The sample was melted six times to ensure homogeneity. The samples were finally wrapped in Ta foil and annealed at 1050 °C for one week in evacuated quartz tubes.

Due to the high vapor pressure of Yb, the $YbNi_2B_2C$ sample was prepared by a solid-state reaction technique. First Ni and B were taken in a 1:1 molecular weight ratio and melted in an arc furnace under flowing argon. Any loss in weight was taken to be due to boron and was accordingly compensated. The ingot was powdered and mixed with an appropriate amount of C powder and small pieces of Yb and the mixture was pelletized. The pellet was sealed in a Mo crucible under an argon atmosphere and the crucible was then sealed in a quartz tube under vacuum. The sealed ampoule was heated to 1250 °C over a period of 24 h and then furnace cooled. The samples were ground and pelletized and the whole procedure was repeated once to get the final product. The pellets had good mechanical strength indicating a good solid-state reaction.

With the exception of Y and Yb, the samples were prepared with the ^{11}B isotope to reduce the unwanted neutron absorption of ^{10}B found in naturally occurring boron. Typically the weight of each sample was 2–5 g. Phase purity of the material was checked by powder x-ray diffraction. The samples were then characterized by a variety of techniques. Resistivity was measured using the four-probe method. Both ac and dc magnetization measurements were employed to look for the superconducting transition and to study the magnetic behavior. Heat-capacity measurements were done using the semiadiabatic heat-pulse technique.

The neutron-diffraction experiments were carried out at the National Institute of Standards and Technology research reactor. The temperature-dependent magnetic diffraction data were obtained on the BT-2 triple-axis spectrometer operated in two-axis mode. A pyrolytic graphite monochromator and filter were employed at a wavelength of 2.351 Å in the usual manner, and the collimation before and after the sample was typically 20′ full width at half maximum. The samples were held in an aluminum cylindrical holder and placed in an ILL-type top loading cryostat to cool the sample from room temperature to temperatures as low as 1.6 K. Lower temperatures were achieved with a cold-finger pumped[3] He cryostat (to 0.3 K). For the highly absorbing Y sample we used a thin flat-plate holder to minimize the effects of absorption, while for the Yb sample we employed a cylindrical annulus.[24] In addition, during the long shutdown of the NIST reactor some data on the Ho, Dy, and Er samples were collected on the HB-3 spectrometer at the Oak Ridge National Laboratory utilizing a similar experimental configuration.

High-resolution powder-diffraction data were obtained on the BT-1 spectrometer at NIST, employing the Cu(311) monochromator and a wavelength of 1.54 Å. The samples were placed in a cylindrical holder made of vanadium, with the exception of the Yb sample which again was put in an aluminum annulus. These data were then used to obtain complete structural refinements for all the samples at room temperature, and at a few selected temperatures below this. Preliminary data were also collected on some of the samples with the HB-4 powder diffractometer at Oak Ridge National Laboratory. However, to facilitate the most direct comparison between the different samples all the refinements reported here were obtained on BT-1. The standard GSAS (Ref. 25) program was used to refine all the structural data, and this program was also used in most cases to refine the magnetic structure when the structure was commensurate.

In cases where just a few magnetic peaks were observed, or the magnetic structure was incommensurate, the integrated intensities of the magnetic and nuclear intensities were obtained by fitting a resolution-limited Gaussian to each observed peak. In this case the intensity for the nuclear reflection is given by[26]

$$I_N = C|F_N(hkl)^2| \frac{m_{hkl} A_{hkl}}{\sin(\theta)\sin(2\theta)}, \tag{1}$$

where C is an instrumental constant, m_{hkl} is the multiplicity of the powder peak with Miller indices hkl, A_{hkl} is the absorption factor, and the nuclear structure factor is given by

$$F_N = \sum_{j=1}^{N} b_j e^{i\tau\cdot\mathbf{r}_j} e^{-W_j} \tag{2}$$

with τ the reciprocal-lattice vector of the Bragg peak hkl, b_j the coherent nuclear scattering amplitude for the jth ion at position $\mathbf{r}_j$ in the unit cell, W_j is the Debye-Waller factor, and the sum is over all atoms in the unit cell. The magnetic intensity is given by the similar expression

$$I_M = C\left(\frac{\gamma e^2}{2mc^2}\right)^2 |F_M|^2 \frac{m_{hkl} A_{hkl}}{\sin(\theta)\sin(2\theta)}, \tag{3}$$

where the constant in parentheses is the neutron-electron dipole coupling constant, and the magnetic structure factor is given by

$$F_M = \sum_{j=1}^{N} (\hat{\tau}\times[\hat{\mathbf{M}}_j\times\hat{\tau}])\langle\mu_j^z\rangle f_j(\tau) e^{i\tau\cdot\mathbf{r}_j} e^{-W_j}, \tag{4}$$

where M_j is the direction of the atomic moment, $\langle\mu_j^z\rangle$ is the ordered moment, and $f_j(hkl)$ is the magnetic form factor. For the magnetic form factors of the rare-earth ions we used the free-ion calculated values.[27] For the incommensurate structures it is convenient to write the magnetic structure factor in terms of the nth Fourier component of the moment μ_j^n at site j,[28]

$$F_M = \sum_{j=1}^{N} \{\mu_j^n - \hat{\tau}[\hat{\tau}\cdot\mu_j^n]\} f_j(\tau) e^{i\tau\cdot\mathbf{r}_j} e^{-W_j}. \tag{5}$$

A model for each spin structure is then developed and least-squares fit to the observed magnetic intensities. The magnetic intensities can then be put on an absolute scale by comparison with the nuclear intensities. We also employed the subtraction technique,[29] whereby the nuclear-diffraction pattern above the ordering temperature is subtracted from the data observed at low temperatures. If there is no significant structural distortion, as is the case for the present systems, and the temperature variation of the lattice parameter is not significant compared to the instrumental resolution, then the

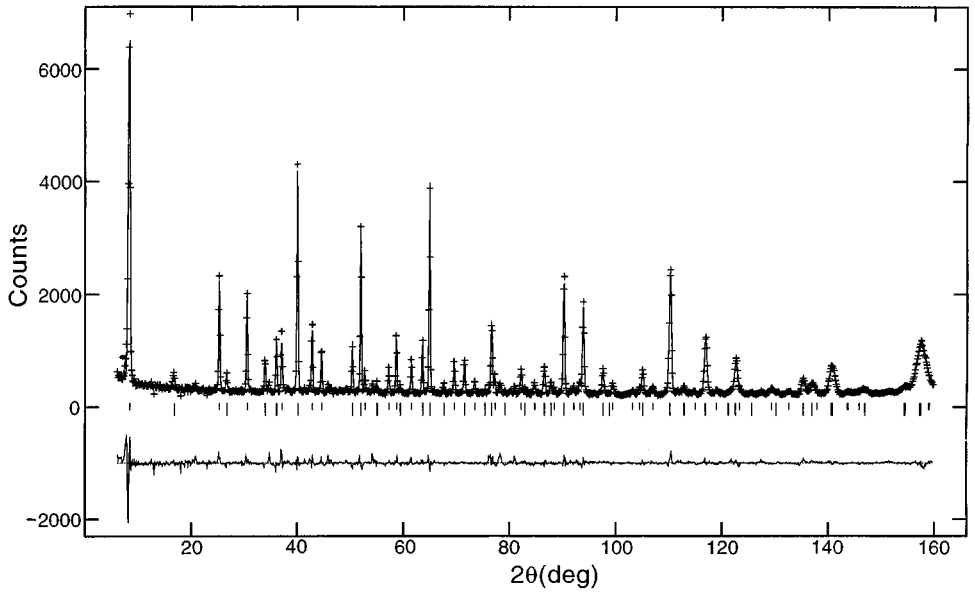

FIG. 1. Diffraction pattern and refinement for $HoNi_2B_2C$ at 1.7 K in the antiferromagnetically ordered (and superconducting) state. The crosses are the experimental data and the solid curve is from the refinement based on the magnetic (short vertical lines) and nuclear (long vertical lines) Bragg peaks. The difference between the model calculation and the observations is shown at the bottom.

nuclear Bragg peaks subtract out leaving only the magnetic Bragg peaks. This is a convenient way to quickly identify the magnetic diffraction pattern.

Equations (3) and (4) show that the intensity of each magnetic Bragg peak is proportional to the square of the ordered moment, and thus the order parameter (or its square) can be readily obtained from the measurements. In principle, one can determine the spatial dimensionality of the system, the number of components of the order parameter (i.e., Ising, xy, Heisenberg, etc.), critical exponents, etc. In practice, however, trying to extract such quantities from powder-diffraction data is typically unwarranted. In the present case we tried fitting a Brillouin function to the sublattice magnetization as a first step. This is in essence a mean-field theory, which certainly will not be correct in detail for most systems. However, we have simply let all the parameters vary (J, T_N, and saturation magnetization) in order to get the best smooth curve through the data and obtain an estimate of T_N. In some cases a mean-field fit did not provide an adequate fit to the data, and then we simply put a smooth curve through the data.

III. CRYSTAL STRUCTURE

We have carried out high-resolution profile refinements for these materials for a range of temperatures at and below room temperature. An example of the data and structural refinement is shown in Fig. 1, which is for $HoNi_2B_2C$ at 1.7 K. This is in the antiferromagnetically ordered state, and the lowest-angle Bragg peak belongs to the (001) antiferromagnetic reflection. The large holmium moment results in magnetic peaks that are comparable in intensity to the nuclear peaks, and thus the results from the refinements are statistically comparable for the nuclear and magnetic structures. In this figure the short vertical lines designate magnetic peaks, while the long vertical lines indicate the positions of the nuclear Bragg peaks. All the RNi_2B_2C ($R=$ Y, Ce, Pr, Nd, Tb, Dy, Ho, Er, Tm, and Yb) samples investigated possess the same body-centered-tetragonal ($I4/mmm$) structure found originally,[4] which is shown in Fig. 2. The structure consists of R-C planes separated by Ni_2B_2 layers stacked along the c axis. The solid curve in Fig. 1 is the fit to the resultant magnetic and nuclear structure, and we see that we obtain a very good fit as indicated at the bottom of the figure, where the difference between the calculated and observed values is given.

In the following section we will discuss the magnetic structures; here we discuss the crystal structure. Above the magnetic ordering temperatures only the nuclear Bragg peaks are present, and the profile refinement technique readily provides the structural parameters as given in Table I. Figure 3 shows the room-temperature lattice parameters as a function of lanthanide radius. We see that the volume of the unit cell increases smoothly with increasing lanthanide radius, as does the basal plane lattice parameter. The c-axis lattice parameter, on the other, shows an anomalous decrease with increasing radius as was observed in the x-ray data.[4]

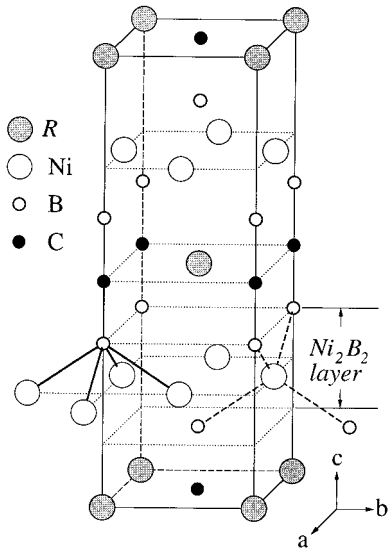

FIG. 2. Body-centered-tetragonal crystal structure ($I4/mmm$) for the RNi_2B_2C series.

TABLE I. Structural parameters, selected interatomic distances (Å), and angles (°) for $R\mathrm{Ni_2B_2C}$ at room temperature. Space group: $I4/mmm$; atomic positions: R (0,0,0), Ni (1/2,0,1/4), B (0,0,z), and C (1/2,1/2,0). B_i: (x,y,z);B_{ii}: $(1/2+x,1/2+y,1/2-z)$.

Atom	Parameter	Ce	Pr	Nd	Tb	Dy	Ho	Er	Tm	Yb
	a (Å)	3.637 83(6)	3.706 6(1)	3.678 0(2)	3.553 61(7)	3.534 20(8)	3.517 7(1)	3.501 9(1)	3.486 6(2)	3.478 2(3)
	c (Å)	10.227 3(2)	9.999 3(3)	10.081 4(4)	10.435 2(3)	10.487 8(3)	10.527 8(3)	10.558 0(4)	10.586 0(5)	10.607(1)
	V (Å^3)	135.346(7)	137.38(3)	136.37(2)	131.777(8)	130.998(8)	130.27(1)	129.48(1)	128.68(2)	128.32(3)
R	B (Å^2)	0.58(3)	0.82(5)	0.52(3)	0.47(3)	0.31(4)	0.27(4)	0.36(4)	0.50(3)	0.6(1)
Ni	B (Å^2)	0.63(2)	0.85(2)	0.77(2)	0.57(2)	0.90(4)	0.60(2)	0.34(2)	0.51(2)	0.7(1)
B	z	0.354 4(1)	0.351 5(2)	0.352 7(2)	0.357 4(2)	0.358 4(3)	0.359 2(2)	0.359 7(2)	0.359 8(2)	0.359 3(8)
	B (Å^2)	0.83(2)	1.03(2)	1.08(3)	0.77(2)	1.21(6)	0.83(3)	0.61(3)	0.68(3)	0.4(2)
C	B (Å^2)	0.71(3)	0.84(3)	0.86(4)	0.85(4)	0.82(1)	0.81(5)	0.21(5)	0.42(3)	1.2(3)
	R_p (%)	4.10	5.03	5.62	5.56	5.99	4.62	5.79	6.23	9.04
	R_{wp} (%)	5.08	6.25	6.73	6.84	7.34	5.66	7.16	7.73	11.79
	χ^2	1.397	1.192	1.115	1.569	1.345	1.274	1.383	1.065	1.065
					Selected interatomic distances (Å) and angles (°)					
R-B		2.972 2(6)	3.012 6(8)	2.994 8(9)	2.920 6(9)	2.907(1)	2.896(1)	2.885(1)	2.887 8(9)	2.877(4)
R-C		2.572 33(4)	2.620 99(7)	2.600 7(1)	2.512 78(5)	2.499 06(6)	2.487 39(7)	2.476 23(7)	2.465 4(1)	2.4594(4)
Ni-B		2.109 2(6)	2.112 8(8)	2.110 4(9)	2.100 5(9)	2.101(2)	2.101(1)	2.100(1)	2.095(1)	2.090(5)
B-C		1.489(1)	1.485(2)	1.485(2)	1.489(2)	1.485(3)	1.483(2)	1.481(2)	1.485(2)	1.492(8)
B_i-Ni-B_{ii}		104.85(3)	103.33(3)	103.93(4)	106.53(4)	107.02(7)	107.41(4)	107.73(5)	107.92(4)	107.9(2)
B_i-Ni-B_i		119.16(6)	122.61(8)	121.24(9)	115.54(8)	114.5(1)	113.68(9)	113.02(9)	112.63(8)	112.6(4)

The only apparent exception to this smooth variation appears to be for Ce, which did not fall on the curve unless we adjusted the radius by admixing Ce^{4+}, suggesting that this is mixed valent. Indeed mixed-valent behavior for Ce has already been suggested.[15] A similar trend is found for the lattice parameters as a function of temperature, as shown in Fig. 4 for the Ho and Ce materials, where we see that a increases with increasing temperature while c decreases. The same trend is found for all the other samples.

We can understand this behavior when the full results of the structural analysis are reviewed. Figure 5 presents some of the relevant bond distances and angles as a function of

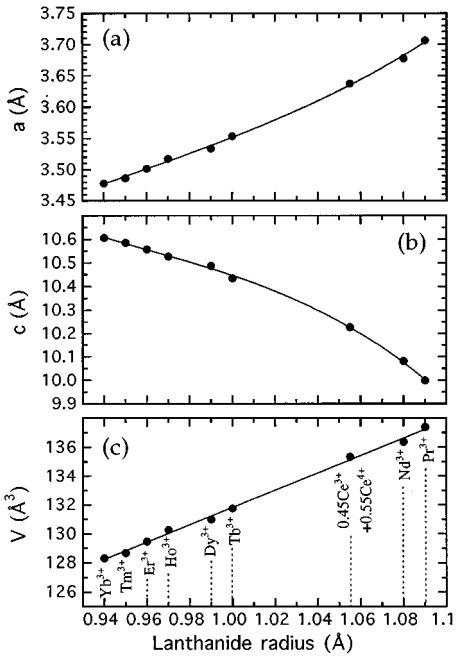

FIG. 3. Room-temperature lattice parameters and unit-cell volume as a function of lanthanide radius.

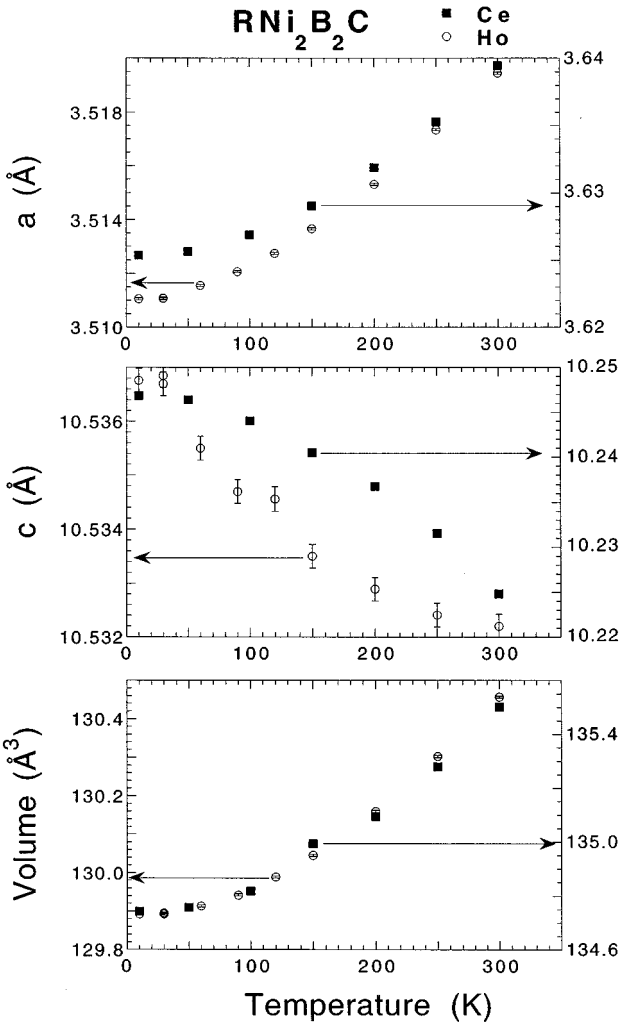

FIG. 4. Lattice parameters and unit-cell volume as a function of temperature for $\mathrm{HoNi_2B_2C}$ and $\mathrm{CeNi_2B_2C}$.

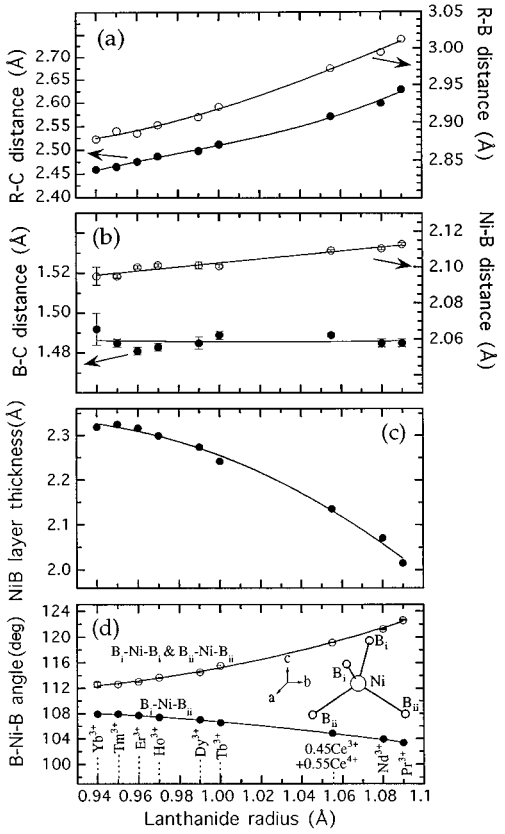

FIG. 5. Bond distances and angles at room temperature as a function of lanthanide radius. Note that the B-C and Ni-B bond lengths do not exhibit much variation with radius, and this forces the Ni-B layer thickness to decrease as the lanthanide radius increases (see text).

lanthanide radius. In Fig. 5(a) we see that for the *R*-C layer, the in-plane basal area increases with increasing radius as required by the data of Fig. 3(a). The B-C bond distance [Fig. 5(b)] along the *c* axis, on the other hand, shows no significant variation with radius, indicating that this bonding is very strong. Thus the *c*-axis layer defined by the B-C-B atoms, with the rare earth in the middle, does not change height as the lanthanide radius (or temperature) is varied, while the basal-plane area changes in the conventional manner. This requires that the *R*-B distance vary in the same manner as the *R*-C distance, as observed [Fig. 5(a)].

The second piece of the puzzle comes from the Ni-B bond distance, which also does not exhibit much variation with lanthanide radius. If the Ni-B separation does not change, then this requires a change in the B-Ni-B bond angles and layer thickness. The atomic displacements observed when the Pr ions are replaced by the smaller Tm ions are shown in Fig. 6. This pulls in the C atoms, and with them go the B atoms. The Ni atoms must also move in, but are then forced downward to maintain the same Ni-B bond distance, which results in an increase in the Ni-B layer thickness and a change in the bond angles as shown in Figs. 5(c)– 5(d).

Finally we note both the magnetic and superconducting properties of these systems are very sensitive to subtle variations in the composition.[23] Thus one of the goals of our crystallographic studies was to establish the correlation between the changes in the crystal structure and/or atomic occupancies, and the changes in the magnetic and superconducting properties that are observed from sample to sample. In particular, we wanted to understand what is controlling the delicate balance between the magnetic structures and the superconducting state in the $HoNi_2B_2C$ system.[30] However, the site occupancies and structure for the $HoNi_2B_2C$ sample measured in the present study were identical within statistical accuracy to the samples investigated previously even though the size of the various magnetic components, and the depth of the reentrant superconducting transition, varied by more than a factor of 2 as discussed below. Therefore within the present accuracy of these profile refinements (Table I) we were unable to identify such a correlation.

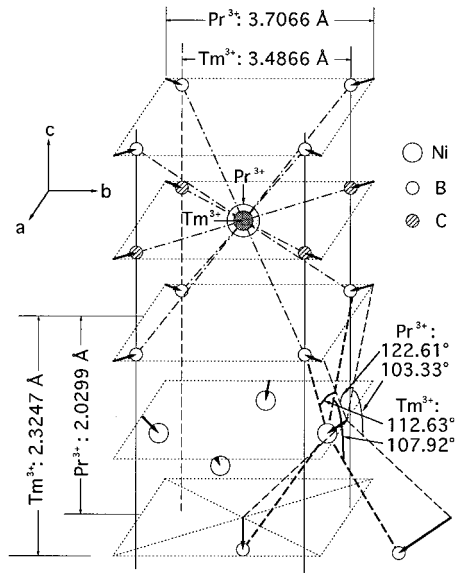

FIG. 6. Atomic displacements that occur when Pr is replaced with the smaller Tm ion.

IV. MAGNETIC ORDERING

We now turn to the presentation of the magnetic structures and phase transitions in this series of materials. For Nd, Pr, Dy, and the ground state of $HoNi_2B_2C$, the magnetic structures are simple commensurate ones. However, for $HoNi_2B_2C$ two different incommensurate modulations are observed at elevated temperatures, where the reentrant superconducting behavior is found. For Tb, Er, and Tm, on the other hand, the magnetic structures are incommensurate throughout the entire temperature range where the magnetic order exists.

A. Pr, Dy, and $HoNi_2B_2C$

The first system to be investigated with neutrons was $HoNi_2B_2C$ because of the doubly reentrant superconducting behavior[14] exhibited by this material.[18] The magnetic scattering observed at low temperatures is shown in Fig. 1. An excellent fit to these data is obtained with the magnetic structure shown in Fig. 7(a). For this structure the moments are coupled ferromagnetically in the (tetragonal) basal plane, forming ferromagnetic sheets, which are then stacked antiferromagnetically along the *c* axis. The wave vector δ de-

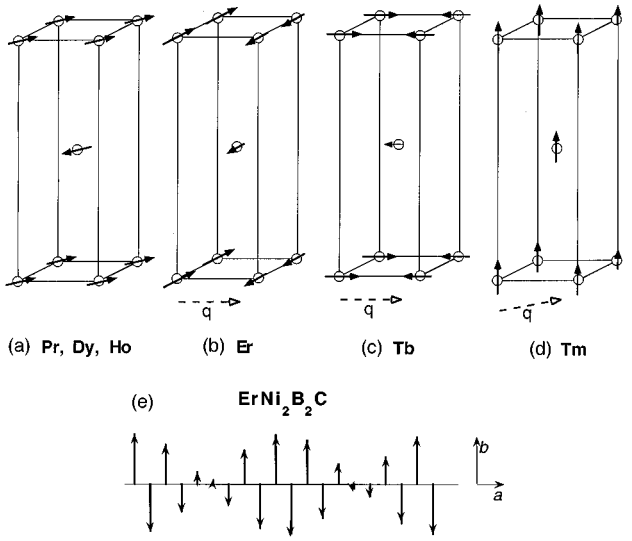

FIG. 7. Magnetic structures observed for (a) Pr, Dy, and Ho at low T, which consists of ferromagnetic sheets of spins in the a-b plane that are coupled antiferromagnetically along the c axis. The wave vector describing the structure is $\delta=[001]$; (b) Er, which is a transversely polarized spin-density-wave with $\delta\|[100]$; (c) Tb, which is a longitudinally polarized spin-density wave with $\delta\|[100]$; (d) Tm, which is a transversely polarized spin-density wave with $\delta\|[110]$; (e) Transverse spin-density wave for the a-axis modulation of $ErNi_2B_2C$, shown over several unit cells.

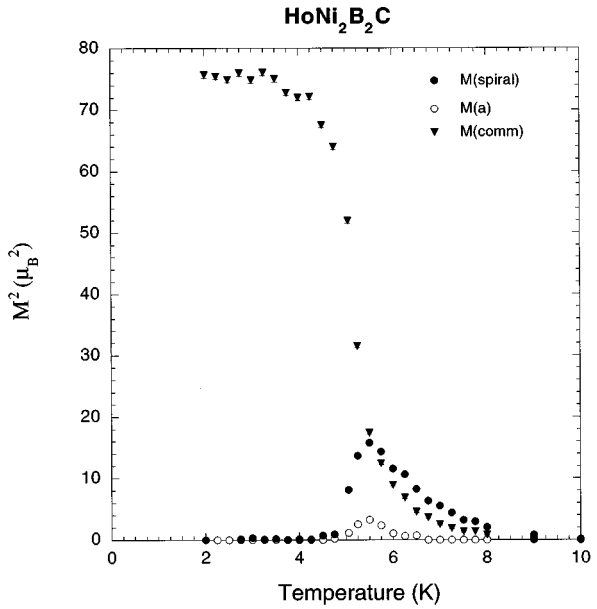

FIG. 8. Intensity of the antiferromagnetic ($M_{\rm comm}$), c-axis spiral ($M_{\rm spiral}$), and a-axis (M_a) magnetic peaks as a function of temperature for $HoNi_2B_2C$. The intensities for the incommensurate magnetic peaks are suppressed below the temperature where the superconducting state reemerges.

scribing this structure is then [001]. The low-temperature magnetic moment we obtain from these data is $(8.62\pm0.06)\mu_B$, with the direction in the a-b plane. The easy direction within the a-b plane cannot be obtained from (zero-field) neutron data, either from powders or single crystals, but magnetization measurements show that the easy axis is the [110] direction.[31] Our refinements based on the data of Fig. 1 indicated that there is no moment along the c axis within the error quoted above, and this result is inconsistent with the c-axis component of the moment reported by Tomy *et al.*[21]

One of the interesting questions in these materials is whether or not the Ni ions carry a magnetic moment of any kind, in analogy with the cuprate systems. There were initial reports of a possible magnetic phase transition in YNi_2B_2C, but no type of magnetic ordering was observed,[28] and it appears now that the Ni by itself is not magnetic.[33] However, in the presence of rare-earth ordering a significant induced moment may be present on the Ni ion,[32] and in our initial work on $ErNi_2B_2C$ (Ref. 28) it was found that including a small induced moment on the Ni site gave a small improvement (at the few percent level in the intensities) to the fit of the data. Our new $ErNi_2B_2C$ data and analysis will be discussed below, but the Er system has a rather complicated incommensurate magnetic structure, and it was clear that a detailed analysis on a material with a simple commensurate magnetic structure would give a more definitive answer. The Ho system is an obvious choice because it has a large ordered moment and little nuclear absorption, but in our earlier studies this could not be adequately addressed because at low T there was still some remnant of the high-temperature spiral incommensurate state present in the scattering, and this complicated the analysis too much when trying to look at this level of detail. For the data on the present sample (Fig. 1), on the other hand, the spiral (and a-axis) incommensurate state is absent at low temperature, and the magnetic scattering was restricted to resolution-limited [001]-type Bragg peaks. We then tried including a series of assumed magnetic structures for the Ni, and in each case the moment refined to zero within statistical error. Therefore we find no evidence for a significant nickel moment in the holmium system, and this turns out to be the case for the other samples in this study as discussed below.

The magnetic order that initially develops in $HoNi_2B_2C$ just below the Néel temperature, on the other hand, shows far more interesting behavior. This system becomes superconducting at $T_c\approx8$ K, while developing long-range magnetic order at about the same temperature.[18–20,30,34] The details of these transitions have already been discussed at some length in the literature, so here we will just briefly review the behavior as it pertains to the results for the present sample. Two types of magnetic peaks initially develop, the [001] commensurate antiferromagnetic structure just described, and an incommensurate spiral state in which these ferromagnetic sheets in adjacent layers along the c axis have a relative orientation of $\sim163.4°$, instead of 180° for the commensurate structure. Figure 8 shows the data for the present sample, where we find that the intensities from both types of Bragg peaks begin to develop at $T_N\approx8.5$ K, and initially grow with decreasing temperature at the same rate. At a temperature of ~6.25 K additional magnetic peaks that correspond to a modulation wave vector of $\delta=[0.55,0,0]$ begin to develop. At ~5 K the superconductivity is reentrant as evidenced by a deep minimum in H_{c2} near 5 K,[14,17] below which the incommensurate spiral locks-in to the commensurate antiferromagnetic structure and the intensities of the a-axis type peaks also decrease to zero. This magnetic lock-in transition then

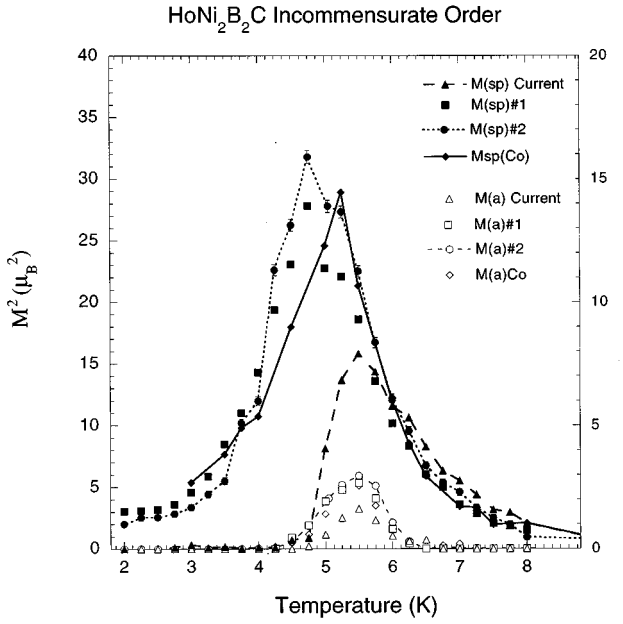

FIG. 9. A comparison of the c-axis incommensurate spiral and a-axis incommensurate intensities for four different $HoNi_2B_2C$ samples; the present work, two previous reentrant superconducting samples, and one where 0.7% Co was substituted for Ni to suppress the superconductivity (Ref. 30). The spiral amplitudes that begin to develop at $T_N \approx 8.5$ K all have the same size and temperature dependence initially, but the lock-in transition occurs at a higher temperature in the present sample. The temperature dependence of the a-axis peak is similar for all the samples, but the intensity for the present sample is almost half the other ones.

permits the return of superconductivity and the coexistence of superconductivity with the commensurate long range antiferromagnetic order at low T.

We have carried out measurements on a number of different $HoNi_2B_2C$ samples, and a comparison of the intensities of the incommensurate peaks is shown in Fig. 9. The intensity for the spiral state develops in each sample at ~ 8.5 K, and the temperature dependence is initially identical for all the samples. However, for the present sample (triangles) the intensity starts to decrease at a considerably higher temperature than for the previous samples studied.[30] The reentrant superconducting anomaly is also considerably smaller for this sample, and this may be correlated with the fact that the spiral amplitude does not grow to as large a value. However, we also note that the a-axis peak intensity is also smaller for the present sample, and clearly more work is needed in order to fully clarify the relationship between these three magnetic components and the superconductivity. In particular, the intensities for the a-axis peaks are too weak to allow the magnetic structure to be solved by powder-diffraction techniques, while it has not been possible to solve this structure by measurements on single crystals[20,34] due to extinction effects and other factors. We remark that within experimental error the ordered magnetic moment at low temperatures is the same for each of the samples, and we have not been able to correlate any differences in the chemical structure with the observed differences in the magnetic and superconducting properties. We also note that the initial ordering temperature of 8.5 K for all the powder samples we have studied is considerably higher than that found for the flux-grown single crystals (~ 7 K),[20,34] but agrees rather well with the results for crystals grown by the floating-zone method.[35] We note that so far it has proved difficult to compare the absolute moments we obtain for the three types of peaks with the single-crystal samples because of the extinction problems encountered with the single crystals.

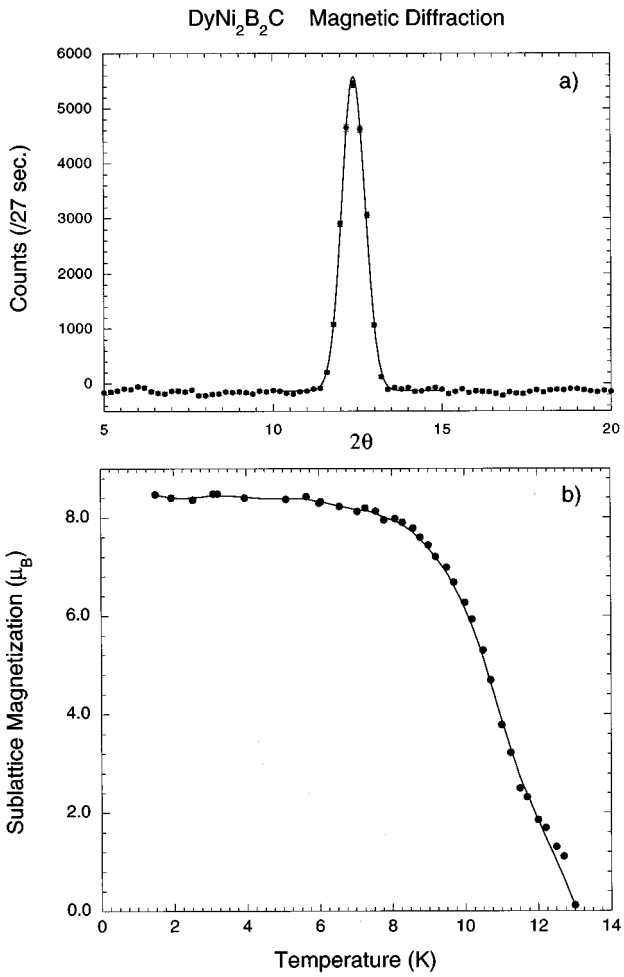

FIG. 10. (a) Magnetic Bragg peak for $DyNi_2B_2C$ at low temperature, and (b) temperature dependence of the sublattice magnetization obtained from the Bragg peak intensity. The solid curve is a guide to the eye.

The magnetic structure for $DyNi_2B_2C$ is identical to the low-T commensurate antiferromagnetic structure of the Ho system, with the moments in the a-b plane being ferromagnetically aligned while the structure is antiferromagnetic along the c axis as shown in Fig. 7(a). Magnetization data indicate that the [110] direction is the easy axis,[36] as is the case for the holmium. The (001) magnetic Bragg peak at 1.7 K is shown in Fig. 10(a). The magnetic signal is identified by utilizing the subtraction technique, where we subtract the data taken well above the ordering temperature from the low-temperature data.[29] We see a resolution-limited Bragg peak indicative of long-range antiferromagnetic order,[37] while the scattering away from the Bragg peak is negative due to the absence of the paramagnetic diffuse scattering in the ordered magnetic state. These data were obtained on the HB-3 spectrometer at Oak Ridge National Laboratory. The structure we

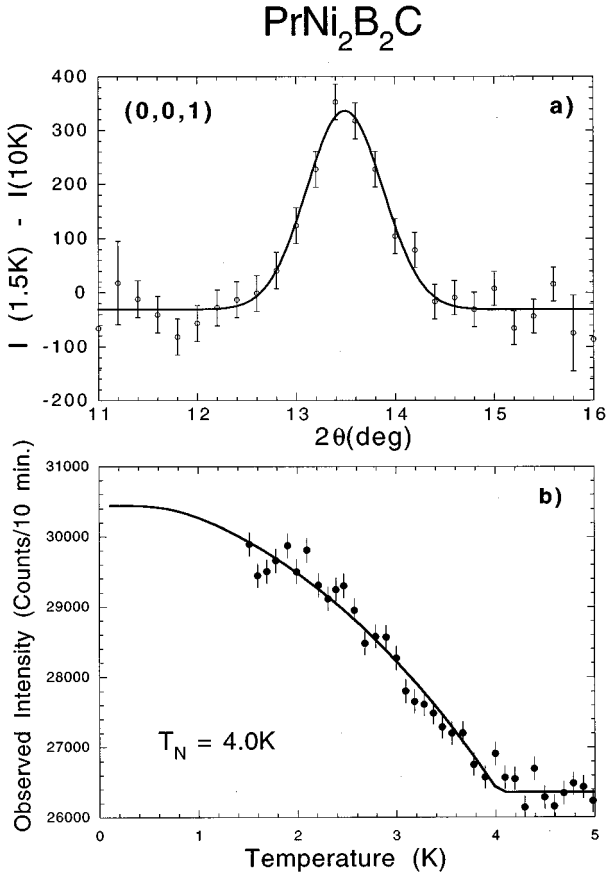

FIG. 11. (a) Magnetic Bragg peak for $PrNi_2B_2C$ at low temperature, and (b) temperature dependence of its intensity. The solid curve is a fit to a Brillouin function.

find is in good agreement with the structure found in single crystals.[38] The ordered moment we obtain from a fit to the complete diffraction pattern (out to a scattering angle of 90° at this wavelength) is $8.47(9)\mu_B$. Including a moment on the Ni site did not provide any improvement in the refinement, and hence we conclude that there is no significant ordered magnetic moment on nickel ions in the Dy material. The temperature dependence of the sublattice magnetization obtained from the (001) peak is shown in Fig. 10(b), and we see that the Dy ions in $DyNi_2B_2C$ order antiferromagnetically at a $T_N \sim 11$ K, which is estimated from the change in the curvature in $M(T)$. There is also clearly some critical scattering and/or a spread in T_N in this sample. The solid curve is a guide to the eye. There are no incommensurate magnetic phases observed in this system.

Initially superconductivity was thought to be absent in Dy, but then a superconducting transition of 6 K, (Ref. 39) was discovered, again emphasizing the strong dependence of the physical properties on composition.[23] The superconducting state is very sensitive to the precise composition of the sample, and is present in some samples while absent in others. If the superconducting state is present then there appears to be little interaction between it and the magnetic order parameter, with the two coexisting to low temperatures as found for $HoNi_2B_2C$.

Finally, we note that the $PrNi_2B_2C$ material also orders with the identical magnetic structure as for Dy, and for Ho in the ground state [Fig. 7(a)]. The observed magnetic scattering at low temperatures is shown in Fig. 11(a). In comparison to the Dy system we see that the scattering is obviously much weaker since the ordered moment will be much smaller than for the Dy [and the intensity is proportional to the square of the moment as shown in Eqs. (3) and (4)]. The ordered moment we obtain is only $0.81(3)\mu_B$, which is considerably smaller than the free-ion value. The intensity of the magnetic order is shown in Fig. 11(b) as a function of temperature. The solid curve is a fit to a Brillouin function, and we obtain an ordering temperature of 4.0(1) K. No superconducting transition has been seen yet in $PrNi_2B_2C$, but its absence may have a different origin in analogy with the cuprate systems. In particular, with the exception of the Pr_2CuO_4 system where the Pr is in an isolated singlet (and hence non-magnetic) crystal-field ground state, none of the Pr-containing cuprates exhibit superconductivity, and this is thought to arise from strong f-electron hybridization effects with the conduction electrons.[40] This is an area that requires further investigation.

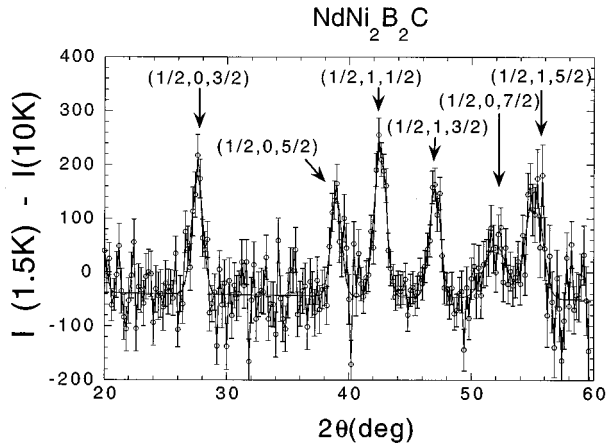

FIG. 12. Magnetic-diffraction pattern obtained on $NdNi_2B_2C$ by subtracting the data at 10 K from the data obtained at 1.5 K.

B. $NdNi_2B_2C$

A portion of the magnetic-diffraction pattern for $NdNi_2B_2C$ is shown in Fig. 12. As for the Pr system, the magnetic Bragg peaks are weak due to the small moment for the light rare earths, but fortunately these peaks may be readily indexed on the basis of the commensurate magnetic structure shown in Fig. 13. The magnetic structure for Nd is then antiferromagnetic along the a axis, with the moment direction along a. The coupling is ferromagnetic along the b axis, while along the c axis one adjacent neighbor is ferromagnetic while the other is antiferromagnetically aligned, doubling the c-axis periodicity. The modulation wave vector is then (1/2, 0, 1/2), with an equivalent domain where $\delta =$ (0, 1/2, 1/2) and the moment direction is along b. This is obviously quite a different structure than the commensurate structure just discussed above for Ho, Dy, and Pr. In particular, note that the bilinear exchange interactions between adjacent planes along the c axis cancel for this spin configuration due to the bcc symmetry, as happens for the Cu order in the 2-1-4 electron superconductors.[41] We observed seven magnetic peaks with nonzero intensity, and the model pro-

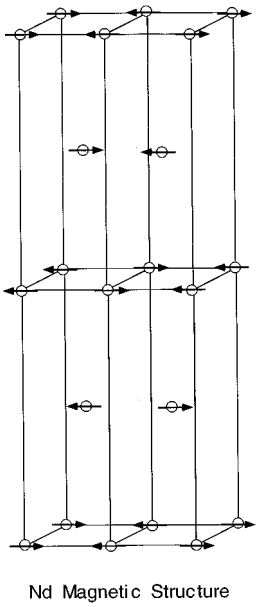

FIG. 13. Magnetic structure of $NdNi_2B_2C$. The spin direction is along the a axis, and this coupling is antiferromagnetic, while the coupling along b is ferromagnetic. Along the c axis one nearest neighbor is aligned antiparallel and one parallel, which requires a doubling of the magnetic unit cell along c.

vided a good fit within statistical errors to the data, with an ordered moment at low temperatures of $2.10(7)\mu_B$. The temperature dependence of the (1/2, 1, 3/2) magnetic Bragg peak is shown in Fig. 14, where the solid curve is a fit of the data to a Brillouin function. The fitted ordering temperature is 4.78(7) K.

C. Er and $TbNi_2B_2C$

For the Er system the superconducting transition occurs at $T_c \sim 11$ K, and superconductivity persists to low temperatures with no reentrant transitions or evidence of strong coupling to the magnetic state. This system has been studied previously by us on powders,[28] and on single crystals by

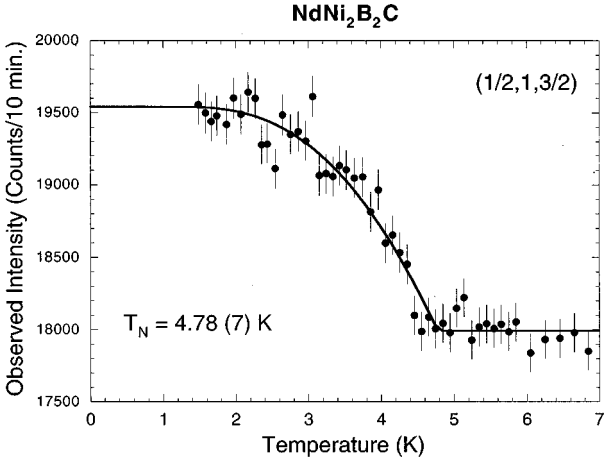

FIG. 14. Temperature dependence of the intensity of the (1/2, 1, 3/2) magnetic Bragg peak in $NdNi_2B_2C$. The solid curve is a fit to a Brillouin function.

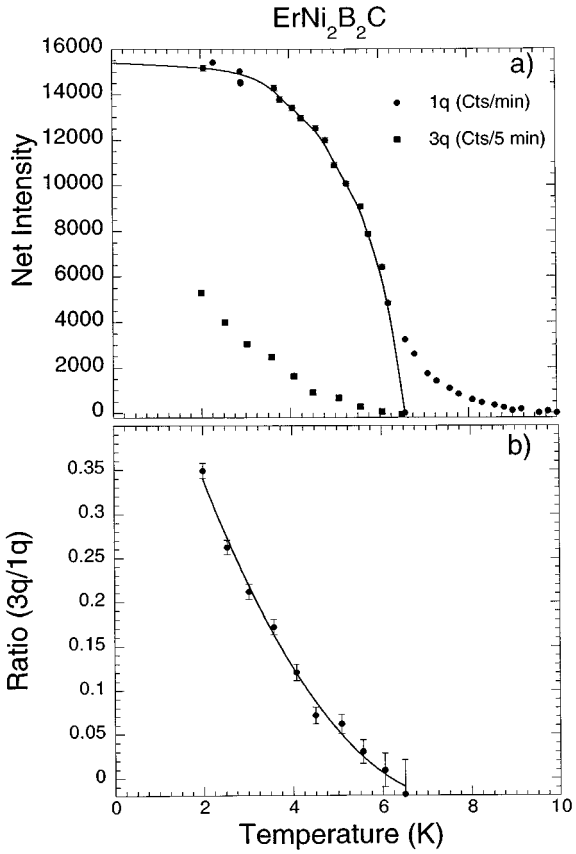

FIG. 15. (a) Intensity of the first and third-order satellite peaks for the spin-density wave in $ErNi_2B_2C$. (b) Ratio of the intensities of these two satellites.

Zarestky *et al.*[42] We found that antiferromagnetic order develops at $T_N = 6.8$ K, with the Er ions forming a transversely polarized, incommensurate spin-density wave state as shown in Fig. 7(b). The modulation wave vector for this state was found to be $\delta = (0.5526, 0, 0)$ (in units of $2\pi/a$) and is approximately temperature independent. The direction of δ is along the a axis (or equivalently along the b axis in this tetragonal system) with the spins directed along b (or a). The variation of the spin-density-wave (SDW) over several periods is shown in Fig. 7(e), which gives a better perspective of what the magnetic structure is in the undistorted SDW state. Note that there appears to be two different waves in the system. One is of short period, and would be a simple antiferromagnet if $\delta = (0.5, 0, 0)$. The second one is a much longer period and describes the modulation away from this simple commensurate state. For $\delta = (0.55, 0, 0)$ this second period is $\delta - 1/2 = 0.05$, or ten times longer than the commensurate antiferromagnetic state.

The staggered magnetization increases smoothly as the temperature is decreased below T_N, and is nonhysteretic. Higher-order harmonics develop at lower temperatures, indicating a squaring-up of the magnetic structure. Figure 15(a) shows the intensity of the primary satellite intensity as a function of temperature for this new sample, along with the temperature dependence of the third-order satellite. The ratio of these two intensities is shown in Fig. 15(b), where we see that the ratio is concave upward as expected when these higher order satellites originate from a distortion of the pure

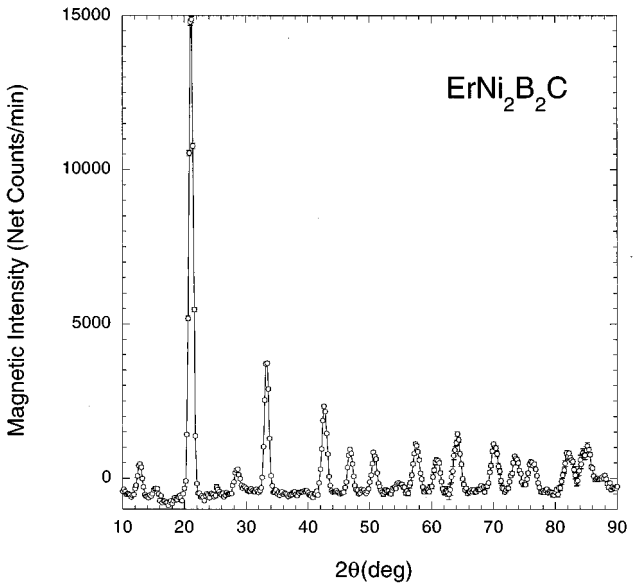

FIG. 16. Low-temperature magnetic-diffraction pattern for $ErNi_2B_2C$. The identification of the peaks is given in Table II.

sine wave as it squares up at low T. This squaring-up of the spin-density wave is expected since a purely sinusoidal spin-density wave cannot be the ground state of a local-moment system because this leaves many of the moments in a partially disordered state. Thus typically the SDW will either square up, or undergo a lock-in transition to a commensurate magnetic structure.[43] No lock-in transition is observed in the present system, and the incommensurate SDW magnetic order and superconductivity are found to coexist over the full temperature range where they are observed, with only a weak interaction between the two.

In our original analysis of the magnetic structure we found that the addition of a small nickel moment in the model improved the fit to the data. However, those data were obtained on a sample containing natural boron, which reduced the statistical precision and introduced systematic errors associated with the large corrections due to the high neutron absorption. We have therefore carried out new measurements on a sample made with ^{11}B so that absorption by the sample is not a problem. We also obtained a more complete magnetic-diffraction pattern to allow a more rigorous comparison between the magnetic structure model[28,44] and the experimental data. Figure 16 shows the magnetic-diffraction pattern for $ErNi_2B_2C$ obtained by subtracting the data at 10 K from the data at 1.5 K. We see that we have a quite complicated pattern arising from the first, third and fifth harmonics of the SDW. All the peaks can be indexed based on this SDW model, and the peak positions and indexing are given in Table II. The calculated and observed intensities are also given for comparison, and from the least-squares fits we obtain the following amplitudes for the sinusoidal moments; $\mu_1 = 9.15(12)\mu_B$, $\mu_3 = 2.77(30)\mu_B$, $\mu_5 = 1.53(40)\mu_B$. If the sine wave becomes a pure square wave at low temperature, then the coefficients in the Fourier series should vary as $1/n$. In this case the amplitude of the square wave is given by $\mu_1(\pi/4)$, which gives a low-temperature Er moment of $7.19\mu_B$. We also tried to include a nickel moment as we did previously, but the refined moment always converged to zero within statistical error. Therefore we do not find any evidence for a significant ordered nickel moment in $ErNi_2B_2C$.

TABLE II. Comparison of calculated and observed magnetic Bragg peak intensities for $ErNi_2B_2C$.

Position (2θ)	Indexing	Multiplicity	Cal. Intensity	Obs. Intensity
12.78°	$\bar{2}00+3q$	4	1 222	1 117(49)
15.26°	$\bar{3}01+5q$	8	520	520(58)
21.10°	q	4	14 750	14 027(151)
	$\bar{1}01+q$	8		
28.56°	$\bar{2}02+3q$	8	967	943(67)
	$\bar{1}01+3q$	8		
33.31°	$002+q$	8	3 904	3 934(69)
42.65°	$\bar{1}10+q$	8	2 750	2 832(72)
	$\bar{1}03+q$	8		
46.82°	$011+q$	16	1 383	1 241(150)
	$\bar{1}10+3q$	8		
	$\bar{1}03+3q$	8		
50.72°	$\bar{1}12+q$	16	1 291	1 337(50)
54.73°	$\bar{3}01+3q$	8	378	505(78)
	$\bar{2}04+3q$	8		
	$\bar{1}12+3q$	16		
57.52°	$\bar{2}00+q$	4	2 049	2 025(77)
	$004+q$	8		
	$\bar{2}13+3q$	16		
60.86°	$013+q$	16	1 295	1 288(72)
64.16°	$\bar{2}02+q$	8	2 064	2 294(96)
	$\bar{1}01+q$	8		
70.18°	$\bar{1}14+q$	16	2 009	2 173(73)
	$\bar{1}05+q$	8		
73.61°	$\bar{2}11+q$	16	1467	1 691(62)
	$\bar{1}01+5q$	8		
	$\bar{3}12+3q$	16		
	$\bar{1}14+3q$	16		
	$002+3q$	8		
	$\bar{1}05+3q$	8		
	$\bar{4}04+5q$	8		
76.23°	$110+q$	8	1 260	1 504(62)
	$103+q$	8		
82.15°	$\bar{2}04+q$	8	1 768	2 111(108)
	$112+q$	16		
	$\bar{2}15+3q$	16		
	$011+3q$	16		
84.99°	$\bar{2}13+q$	16	1 898	2 931(150)
	$\bar{2}06+3q$	8		
	$\bar{1}10+5q$	8		
	$\bar{1}03+5q$	8		
	$015+q$	16		
	$\bar{2}26+3q$	16		
	$\bar{3}21+5q$	16		
87.70°	$\bar{1}21+q$	16	696	840(68)
	$020+q$	8		
	$006+q$	8		

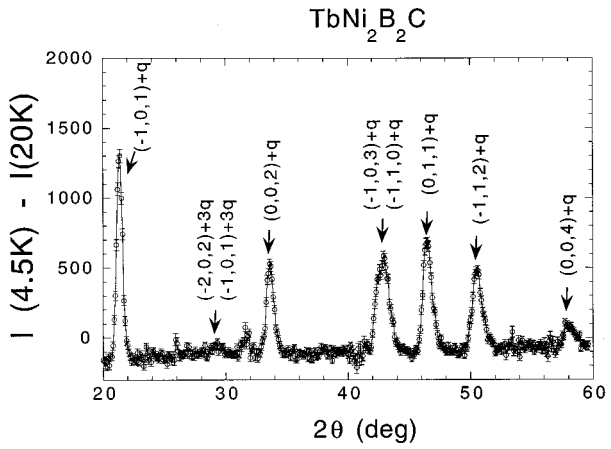

FIG. 17. Low-temperature magnetic-diffraction pattern for $TbNi_2B_2C$.

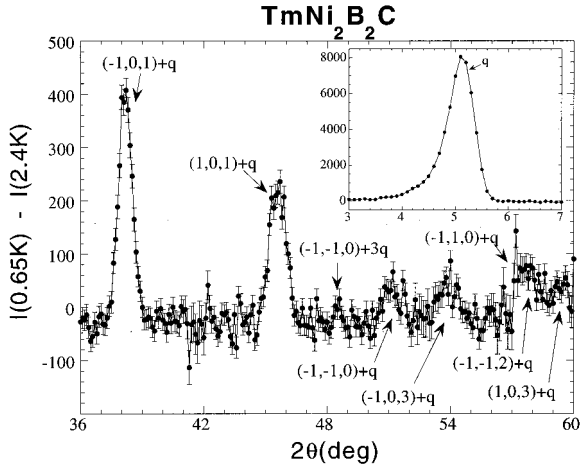

FIG. 19. Low-temperature magnetic-diffraction pattern for $TmNi_2B_2C$.

The low-temperature magnetic-diffraction pattern for $TbNi_2B_2C$ is shown in Fig. 17. This pattern may also be indexed with a model of a SDW along the a axis, with a modulation wave vector $\delta=(0.555,0,0)$ which is very similar in magnitude to Er. The positions of these satellites are in good agreement with the positions reported by other groups on single crystals.[45] However, it is evident that the observed diffraction pattern appears to be quite a bit simpler than for Er, and the reason for this is that the SDW is longitudinally polarized as shown in Fig. 7(c), rather than transversely polarized as for the Er case. In the case of longitudinal polarization the moment direction is parallel to δ, and then the orientation factor (triple cross product) in Eq. (4) results in a number of peaks having vanishing intensity. We also see evidence for a higher-order satellite, which is unobservable at higher temperatures, indicating that the SDW has squared up. We find $\mu_1=9.90(36)\mu_B$ from the least-squares fit. Assuming a square-wave structure at low temperatures, we obtain a value for the ordered moment of $\langle\mu\rangle=7.78(28)\mu_B$. We also remeasured the first and third-order satellite peaks at 1.7 and 7 K to determine if the $3q$ peak is associated with a squaring up of the structure. We found essentially the same intensity for the first-order satellite, while for the third-order satellite we obtain $\mu_3=2.28(13)\mu_B$ at 1.7 K, and $\mu_3=1.65(15)\mu_B$ at 7 K.

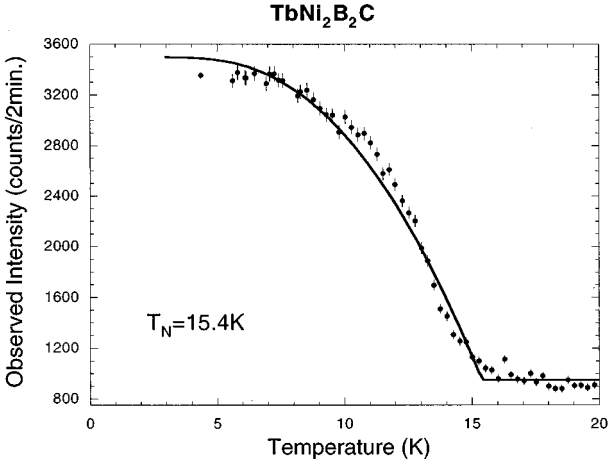

FIG. 18. Temperature dependence of the magnetic Bragg peak for $TbNi_2B_2C$.

The temperature dependence of the intensity of the lowest-angle magnetic Bragg peak is shown in Fig. 18. The antiferromagnetic ordering temperature is 15.4(3) K. There is also an anomaly in the temperature dependence at around 10 K. This may be associated with a small ferromagnetic component as observed in magnetization measurements on single crystals at 8 K,[46] or to a transition at 5 K identified as a spin-reorientation transition.[47] A similar transition has been identified recently in $ErNi_2B_2C$,[36] but we do not observe any effects of such a transition in the present powder measurements on that sample. The positions of the peaks in our diffraction pattern were measured at a series of temperatures both above and below 10 K, and there is no significant variation in the positions of the magnetic peaks. Hence the modulation wave vector does not vary significantly with temperature. No superconductivity has yet been found in the $TbNi_2B_2C$ system, and its absence may be linked to this additional ferromagnetic component. However, more work will be needed before this link can be established unambiguously.

D. $TmNi_2B_2C$

Another rare earth that exhibits an incommensurate magnetic state is $TmNi_2B_2C$. This system becomes superconducting at 11 K while it orders magnetically at only 1.5 K.[48,49] However, the modulated magnetic structure is completely different from any of the other systems. The modulation wave vector is in the a-b plane, but is along the [110] direction, with a temperature-independent magnitude of 0.24 $Å^{-1}$, giving $\delta=$ (0.093, 0.093, 0). The direction of the magnetic moment, on the other hand, is along the c axis. Thus the magnetic structure is a transversely polarized SDW state as for $ErNi_2B_2C$, but with the spins pointing along the c axis as shown in Fig. 7(d) rather than in the a-b plane. Figure 19 shows the magnetic diffraction pattern observed at low temperature. Because the incommensurate wave vector is small in magnitude, the first-order peak has strong intensity due to the $\sin(\theta)\sin(2\theta)$ factor in Eq. (3), while the shape

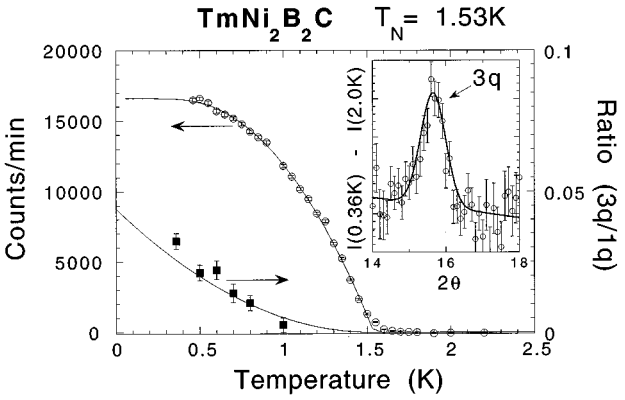

FIG. 20. Temperature dependence of the magnetic Bragg peak intensity associated with the incommensurate ordering in $TmNi_2B_2C$. The modulation wave vector for this material is in the [1,1,0] direction, which is unique for this class of materials. The $3q$ satellite peak observed at low temperatures is shown in the inset, and indicates that the magnetic structure has squared-up while remaining incommensurate. The temperature dependence of the ratio of the third-order to first order intensities is also shown.

is asymmetric due to the contribution of the vertical resolution at this small a scattering angle. Again we see a $3q$ peak, indicating that the SDW squares up at low temperature, with the magnetic structure remaining incommensurate. We obtained $\mu_1 = 4.81(18)\mu_B$ and $\mu_3 = 0.93(19)\mu_B$ at this temperature, and assuming a square wave at low T this gives an ordered moment of $3.78\mu_B$. Figure 20 shows the development of the long-range order in this material, where we see that we have strong intensity and a nicely defined phase transition at 1.53 K. The inset shows the magnetic intensity for the lowest-angle $3q$ peak, and the temperature dependence of the ratio of the first- to third-order intensities is also shown as a function of temperature. This incommensurate long-range magnetically ordered state coexists with superconductivity.

Recently magnetic ordering has been reported independently for $TmNi_2B_2C$.[50] The incommensurate wave vector they found is the same as that reported here, although they did not report the observation of any higher-order satellites, or a measurement of the order parameter.

E. Y, Ce, and $YbNi_2B_2C$

Finally, we note that we have carried out low-temperature diffraction measurements on the YNi_2B_2C, $CeNi_2B_2C$, and $YbNi_2B_2C$ materials, but no evidence of any magnetic order was observed. The Y system is of course superconducting at 15.5 K, while no superconductivity has been found in either the Ce or Yb systems. The Ce system may have mixed-valent behavior, which could explain the absence of superconductivity, while the Yb material exhibits some moderate heavy-fermion effects.[51]

V. DISCUSSION

A summary of the type of magnetic structure, the spin direction, ordered moment, and magnetic transition temperature obtained in the present study is given in Table III, along with the transition temperature for those systems that become superconducting. We have also included the magnetic properties for the Gd compound for completeness, which was investigated via magnetic x-ray diffraction[16] due to the very large neutron absorption cross section for Gd. We see that these materials exhibit quite a variety of magnetic structures. About half the materials—Pr, Nd, Dy, and Ho—have commensurate antiferromagnetic structures, and for the Dy and Ho this simple antiferromagnetic ground state coexists with superconductivity. The Gd, Tb, Er, Tm, on the other hand, form incommensurate magnetic structures. The Er and Tm materials also exhibit superconductivity, which again coexists with the long-range magnetic order.

TABLE III. The magnetic structure, ordered moment, Néel temperature, and modulation wave vector determined in the present neutron-scattering study for the RNi_2B_2C systems. The superconducting transition temperature is also given for the materials that are superconducting. The Gd system was investigated by magnetic x-ray scattering (Ref. 16) because of the high absorption of Gd for neutrons, and is included for completeness. For the ground-state magnetic structures of Ho and Dy the neutron measurements cannot distinguish the easy axis in the a-b-plane, but magnetization measurements indicate that the easy axis is [110] (Refs. 31 and 36). Comparisons with other neutron and x-ray work are given in the text.

R	T_N	T_c	Structure	δ	$\mu(\mu_B)$	Direction
Pr	4.0		Comm AF	0, 0, 1	0.81(9)	a-b
Nd	4.8		Comm AF	1/2, 0, 1/2	2.10(7)	a
Gd	19		a axis	0.55,0,0	7	b [a]
Tb	15		a axis	0.555,0,0	7.78(28)	a
Dy	10.6	6	Comm AF	0,0,1	8.47(9)	110
Ho	8.5	8	c-axis spiral	0,0,0.91	6.7	110
	6.3		a axis	0.55,0,0	?	?
	5	5	Comm AF	0,0,1	8.62(6)	a-b
Er	6.8	11	a-axis SDW	0.5526,0,0	7.19(10)	b
Tm	1.53	11	SDW	0.093,0.093,0	3.78(14)	c
Yb, Ce						

[a]The initial ordering for Gd occurs at 19 K, into a transversely polarized spin-density-wave state very similar to the Er system. At 14 K a c-axis component to the moment develops (unlike the Er) (Ref. 16). The ground-state moment was not determined in this system, but it is presumed to be $7\mu_B$ since Gd is a spin-only ion.

From the point of view of the magnetic ordering in these materials, the wide variety and complicated nature of the magnetic structures is reminiscent of the elemental rare earths,[22] and strongly suggests that the exchange in the present materials must be mediated by RKKY interactions. In this case the magnetic structure is controlled by the conduction electron susceptibility, and the maximum in the conduction electron susceptibility would then have to vary from material to material to explain all the observed magnetic structures. As a first step in understanding the nature of the exchange interactions in these systems, random-phase approximation-type calculations of the enhanced susceptibility, based on local-density approximation band structures, have been carried out for $LuNi_2B_2C$.[52] The susceptibility shows a maximum at $\delta = (0.6,0,0)$ along the a-axis direction, which is close to the modulation wave vector observed in a number of the materials. However, more sophisticated

calculations, with the inclusion of matrix elements, are needed. In particular, it will be interesting to determine if the maximum in the conduction electron susceptibility varies with the rare earth in such a way as to provide an explanation for the full range of magnetic structures observed in this class of materials.

The richest behavior both for the magnetism and superconductivity is exhibited by the Ho material, which initially forms a commensurate antiferromagnetic structure along with two incommensurate modulation wave vectors along a and along c (see Table III). In the same temperature regime the material is also developing superconductivity. The holmium material is known to be particularly sensitive to variations in composition,[23] and it appears that at least some of the states occur in different regions of the sample. In particular, in regions where the commensurate antiferromagnetic state initially forms there is probably a simple coexistence with superconductivity.[30] In regions where the incommensurate magnetism develops, though, this is detrimental to the superconducting state, and forces the system to be reentrant or nearly reentrant around 5 K. The magnetic system then locks-in to the commensurate antiferromagnetic structure, whereby the superconducting state recovers and these two cooperative states coexist to low temperatures.

The holmium magnetic structure for the c-axis modulation corresponds to a spiral along the c axis.[18,19,30] For a pure spiral there will be no higher-order satellite peaks in the diffraction pattern, and none was observed in the powder-diffraction experiments. However, including a fourfold anisotropy in the a-b plane should produce some bunching of the moments, and this will give rise to (typically small) higher-order satellite peaks,[28,44] and such peaks have been observed in single-crystal measurements.[20,35] For a SDW-type structure such as observed in Gd, Tb, Er, and Tm, on the other hand, the magnetic structure squares-up at low temperatures, as evidenced by the development of strong higher-order satellite peaks that are easily observed in the powder-diffraction pattern. The SDW structures in the Gd, Tb, Er, and Tm materials remain incommensurate over the full temperature range where they are ordered magnetically. An alternative possibility to the squaring up is that a lock-in transition to a commensurate magnetic structure occurs, and this may be the case for the a-axis structure in the Ho material. The magnetic structure for this a-axis modulation has not been solved yet, but it is clear that the structure locks-in to the commensurate antiferromagnetic structure, which is the ground state for the system. There is still an overall question about whether the magnetic structures associated with the a-axis modulations in all these systems are coexistent or competing with the formation of Cooper pairs. However, since Er is a superconductor while Gd and Tb are not, it is clear that if there is a strong competition, it must arise not from the value of δ itself but from the nature of the polarization of the SDW. This is clearly an area where more work is needed.

ACKNOWLEDGMENTS

We would like to thank Bryan Chakoumakos, Jaime Fernandez-Baca, and Brent Taylor for their generous assistance while we were visiting Oak Ridge National Laboratory, managed by Lockheed Martin Energy Research Corporation for the U.S. Department of Energy under Contract No. DE-AC05-96OR22464. Research at the University of Maryland is supported in part by NSF, DMR 93-02380. Research at CNRS and TIFR is supported in part by the Indo-French Contract No. FEFIPRA 509-IRA.

[1] R. Nagarajan, C. Mazumdar, Z. Hossain, S. K. Dhar, K. V. Gopalakrishnan, L. C. Gupta, C. Godart, B. D. Padalia, and R. Vijayaraghavan, Phys. Rev. Lett. **72**, 274 (1994).

[2] R. J. Cava, H. Takagi, B. Batlogg, H. W. Zandbergen, J. J. Krajewski, W. F. Peck, Jr., R. B. van Dover, R. J. Felder, T. Siegrist, K. Mizuhahi, J. O. Lee, H. Eisaki, S. A. Carter, and S. Uchida, Nature (London) **367**, 146 (1994).

[3] R. J. Cava, H. Takagi, H. W. Zandbergen, J. J. Krajewski, W. F. Peck, Jr., T. Siegrist, B. Batlogg, R. B. van Dover, R. J. Felder, K. Mizuhashi, J. O. Lee, H. Eisaki, and S. Uchida, Nature (London) **367**, 252 (1994).

[4] T. Siegrist, H. W. Zandbergen, R. J. Cava, J. J. Krajewski, and W. F. Peck, Jr., Nature (London) **367**, 254 (1994).

[5] L. F. Mattheiss, Phys. Rev. B **49**, 13 279 (1994); W. E. Pickett and D. J. Singh, Phys. Rev. Lett. **72**, 3702 (1994); L. F. Mattheiss, T. Siegrist, and R. J. Cava, Solid State Commun. **91**, 587 (1994); R. Coehoorn, Physica C **228**, 5671 (1994); L. F. Mattheiss, Phys. Rev. B **47**, 8224 (1993).

[6] D. D. Lawrie and J. P. Franck, J. Supercond. **8**, 591 (1995).

[7] See, for example, M. Xu, P. C. Canfield, J. E. Ostenson, D. K. Finnemore, B. K. Cho, Z. R. Wang, and D. C. Johnston, Physica C **227**, 321 (1994); S. A. Carter, B. Batlogg, R. J. Cava, J. J. Krajewski, W. F. Peck, Jr., and H. Tagaki, Phys. Rev. B **50**, 4216 (1994).

[8] H. Schmidt, M. Müller, and H. F. Braun, Physica **235-240**, 779 (1994).

[9] H. G. Smith, in *Superconductivity in d- and f-Band Metals*, edited by D. H. Douglass (AIP, New York, 1972).

[10] P. Dervenagas, M. Bullock, J. Zarestky, P. Canfield, B. K. Cho, B. Harmon, A. I. Goldman, and C. Stassis, Phys. Rev. B **52**, R9839 (1995).

[11] H. Kawano, H. Yoshizawa, H. Takeya, and K. Kadowaki, Phys. Rev. Lett. **77**, 4628 (1996).

[12] For a thorough review of many aspects of magnetic superconductors see, *Topics in Current Physics*, edited by Ø. Fischer and M. B. Maple (Springer-Verlag, New York, 1983), Vols. 32 and 34.

[13] See, for example, *High Temperature Superconductors*, edited by J. W. Lynn (Springer-Verlag, New York, 1990), Chap. 8, p. 268.

[14] H. Eisaki, H. Takagi, R. J. Cava, K. Mizuhashi, J. O. Lee, B. Batlogg, J. J. Krajewski, W. F. Peck, Jr., and S. Uchida, Phys. Rev. B **50**, 647 (1994).

[15] L. C. Gupta, R. Nagarajan, Z. Hossain, C. Mazumdar, S. K. Dhar, C. Godart, C. Levy-Clement, B. D. Padalia, and R. Vijayaraghavan, J. Magn. Magn. Mater. **140-144**, 2053 (1995); M. E. Massalami, S. L. Bud'ko, B. Giordanengo, and E. M. Baggio-Saitovitch, Physica C **224**, 41 (1995).

[16] C. Detlefs, A. I. Goldman, C. Stassis, P. C. Canfield, B. K. Cho,

J. P. Hill, and D. Gibbs, Phys. Rev. B **53**, 6355 (1996).
[17] P. C. Canfield, B. K. Cho, D. C. Johnston, D. K. Finnemore, and M. F. Hundley, Physica C **230**, 397 (1994); M. S. Lin, J. H. Shieh, Y. B. You, W. Y. Guan, H. C. Ku, H. D. Yang, and J. C. Ho, Phys. Rev. B **52**, 1181 (1995); M. El Massalami and E. M. Baggio-Saitovitch, J. Magn. Magn. Mater. **153**, 97 (1996).
[18] T. E. Grigereit, J. W. Lynn, Q. Huang, A. Santoro, R. J. Cava, J. J. Krajewski, and W. F. Peck, Jr., Phys. Rev. Lett. **73**, 2756 (1994).
[19] Q. Huang, A. Santoro, T. E. Grigereit, J. W. Lynn, R. J. Cava, J. J. Krajewski, and W. F. Peck, Jr., Phys. Rev. B **51**, 3701 (1995); T. E. Grigereit, J. W. Lynn, R. J. Cava, J. J. Krajewski, and W. F. Peck, Jr., Physica C **248**, 382 (1995).
[20] A. I. Goldman, C. Stassis, P. C. Canfield, J. Zarestky, P. Dervenagas, B. K. Cho, D. C. Johnston, and B. Sternlieb, Phys. Rev. B **50**, R9668 (1994).
[21] C. V. Tomy, L. J. Chang, D. McK. Paul, N. H. Anderson, and M. Yethiraj, Physica B **213-214**, 139 (1995).
[22] See, for example, W. C. Koehler, in *Magnetic Properties of Rare Earth Metals*, edited by R. J. Elliott (Plenum, New York, 1972), p. 81.
[23] H. Schmidt, M. Weber, and H. F. Braun, Physica C **246**, 177 (1995); **256**, 393 (1996).
[24] N. Rosov and J. W. Lynn (private communication).
[25] A. C. Larson and R. B. Von Dreele, *General Structure Analysis System*, Report No. LAUR-86-748, Los Alamos National Laboratory, Los Alamos, NM 87545 (1990).
[26] G. E. Bacon, *Neutron Diffraction* (Clarendon, Oxford, 1975).
[27] M. Blume, A. J. Freeman, and R. E. Watson, J. Chem. Phys. **37**, 1245 (1953).
[28] S. K. Sinha, J. W. Lynn, T. E. Grigereit, Z. Hossain, L. C. Gupta, R. Nagarajan, and C. Godart, Phys. Rev. B **51**, 681 (1995).
[29] H. Zhang, J. W. Lynn, W.-H. Li, T. W. Clinton, and D. E. Morris, Phys. Rev. B **41**, 11 229 (1990).
[30] J. W. Lynn, Q. Huang, A. Santoro, R. J. Cava, J. J. Krajewski, and W. F. Peck, Jr., Phys. Rev. B **53**, 802 (1996).
[31] B. K. Cho, B. N. Harmon, D. C. Johnston, and P. C. Canfield, Phys. Rev. B **53**, 2217 (1996).
[32] D. R. Sanchez, H. Micklitz, M. B. Fontes, S. L. Bud'ko, and E. Baggio-Saitovitch, Phys. Rev. Lett. **76**, 507 (1996).
[33] B. J. Suh, F. Borsa, D. R. Torgeson, B. K. Cho, P. C. Canfield, D. C. Johnston, J. Y. Rhee, and B. N. Harmon, Phys. Rev. B **53**, R6022 (1996).
[34] J. P. Hill, B. J. Sternlieb, D. Gibbs, C. Detlefs, A. I. Goldman, C. Stassis, P. C. Canfield, B. K. Cho, Phys. Rev. B **53**, 3487 (1996).
[35] H. Kawano *et al.* (private communication).
[36] P. C. Canfield, S. L. Bud'ko, and B. K. Cho (unpublished).
[37] Preliminary results have been reported, in J. W. Lynn, Q. Huang, S. K. Sinha, Z. Hossain, L. C. Gupta, R. Nagarajan, and C. Godart, Physica B **224**, 66 (1996).
[38] P. Dervenagas, J. Zarestky, C. Stassis, A. I. Goldman, P. C. Canfield, and B. K. Cho, Physica B **212**, 1 (1995); C. V. Tomy, L. J. Chang, D. McK. Paul, N. H. Andersen, and M. Yethiraj, Physica B **224**, 116 (1996).
[39] C. V. Tomy, G. Balakrishnan, and D. McK. Paul, Physica C **248**, 349 (1995); B. K. Cho, P. C. Canfield, and D. C. Johnston, Phys. Rev. B **52**, R3844 (1995); M. S. Lin, J. H. Shieh, Y. B. You, Y. Y. Hsu, J. W. Chen, S. H. Lin, Y. D. Yao, J. C. Ho, and H. C. Ku, Physica C **249**, 403 (1995); C. V. Tomy, M. R. Lees, L. Afalfiz, G. Balakrishnan, and D. Mck. Paul, Phys. Rev. B **52**, 9186 (1995); Z. Hossain, R. Nagarajan, L. C. Gupta, S. K. Dhar, C. Godart, and R. Vijayaraghavan, Physica B **223-224**, 99 (1996).
[40] For a recent review see J. W. Lynn, J. Alloys Compounds (to be published).
[41] See, for example, S. Skanthakumar, J. W. Lynn, J. L. Peng, and Z. Y. Li, Phys. Rev. B **47**, 6173 (1993).
[42] J. Zarestky, C. Stassis, A. I. Goldman, P. C. Canfield, P. Dervenagas, B. K. Cho, and D. C. Johnston, Phys. Rev. B **51**, 678 (1995).
[43] See, for example, J. Rossat-Mignod, in *Methods of Experimental Physics*, edited by K. Sköld and D. L. Price (Academic, Orlando, 1987), Vol. 23 C, Chap. 19.
[44] In Eq. (4) of Ref. 28, the correct expression for model (1) is obtained by replacing the factor $[1-\hat{Q}_y^2]$ by $[1+\hat{Q}_z^2]$, and not $[1+\hat{Q}_z^4]$ as indicated in the text.
[45] P. Dervenagas, J. Zarestky, C. Stassis, A. I. Goldman, P. C. Canfield, and B. K. Cho, Phys. Rev. B **53**, 8506 (1996).
[46] B. K. Cho, P. C. Canfield, and D. C. Johnston, Phys. Rev. B **53**, 8499 (1996).
[47] C. V. Tomy, L. A. Afalfiz, M. R. Lees, J. M. Martin, D. McK. Paul, and D. T. Adroja, Phys. Rev. B **53**, 307 (1996).
[48] B. K. Cho, M. Xu, P. C. Canfield, L. L. Miller, and D. C. Johnston, Phys. Rev. B **52**, 3676 (1995).
[49] J. W. Lynn, Q. Huang, S. K. Sinha, Z. Hossain, L. C. Gupta, R. Nagarajan, and C. Godart, J. Appl. Phys. **79**, 5857 (1996).
[50] L. J. Chang, C. V. Tomy, D. McK. Paul, and C. Ritter, Phys. Rev. B **54**, 9031 (1996).
[51] S. K. Dhar, R. Nagarajan, Z. Hossain, C. Godart, L. C. Gupta, and R. Vijayaraghavan, Solid State Commun. **98**, 985 (1996).
[52] J. Y. Rhee, X. Wang, and B. N. Harmon, Phys. Rev. B **51**, 15 585 (1995).